

πN scattering in relativistic baryon chiral perturbation theory revisited

J. M. Alarcón¹, J. Martín Camalich^{2,3}, J. A. Oller¹ and L. Alvarez-Ruso^{2,4}

¹*Departamento de Física. Universidad de Murcia. E-30071, Murcia. Spain*

²*Departamento de Física Teórica and IFIC, Universidad de Valencia-CSIC, E-46071 Spain*

³*Department of Physics and Astronomy, University of Sussex, BN1 9QH, Brighton, UK*

⁴*Centro de Física Computacional. Departamento de Física. Universidade de Coimbra, Portugal*

Abstract

We have analyzed pion-nucleon scattering using the manifestly relativistic covariant framework of Infrared Regularization up to $\mathcal{O}(q^3)$ in the chiral expansion, where q is a generic small momentum. We describe the low-energy phase shifts with a similar quality as previously achieved with Heavy Baryon Chiral Perturbation Theory, $\sqrt{s} \lesssim 1.14$ GeV. New values are provided for the $\mathcal{O}(q^2)$ and $\mathcal{O}(q^3)$ low-energy constants, which are compared with previous determinations. This is also the case for the scattering lengths and volumes. Finally, we have unitarized the previous amplitudes and as a result the energy range where data are reproduced increases significantly.

1 Introduction

Pion-nucleon scattering is a fundamental process involving the lightest meson and baryon. Therefore, at low energies it is amenable to be studied by the low-energy effective field theory of QCD, Chiral Perturbation Theory (CHPT) [1, 2], which takes into account both the spontaneous as well as the explicit breaking of chiral symmetry in strong interactions. While the baryon field transforms linearly under the chiral group the pions do non-linearly [3]. A first step in extending CHPT to the systems with baryon number one was undertaken in ref. [4]. Contrary to standard CHPT, it was established that due to the presence of the large nucleon mass, loops do not respect the chiral power counting, and the lower order counterterms are renormalized because of higher order loops. The power counting was recovered by applying Heavy Baryon CHPT (HBCHPT) [5], where the heavy components of the baryon fields are integrated out [6, 7] so that manifest Lorentz invariance is lost. On the other hand, for some loop functions the expansion in inverse powers of the nucleon mass and the loop integration do not commute so that the non-relativistic expansion does not converge [8, 7]. The recovery of the power counting, while keeping manifest Lorentz invariance, was achieved by the Infrared Regularization method (IR) [8], based on the ideas in ref. [9]. IR was extended to the multi-nucleon sector [10] and to multi-loop diagrams [11]. Another relativistic approach to baryon CHPT is the so-called extended-on-mass-shell (EOMS) renormalization scheme [12, 13]. The latter is based on removing explicitly the power counting breaking terms appearing in the loop integrals in dimensional regularization since they are re-absorbed by the finite set of low-energy counterterms up to the order the calculation is performed. For a recent review on baryon CHPT see ref. [14].

Here we focus on the application of IR CHPT methods to low-energy pion-nucleon scattering. In HBCHPT there is already an extensive list of detailed calculations with several degrees of precision. In refs. [15, 9, 16] an $\mathcal{O}(q^3)$ calculation is performed, with the additional inclusion of the $\Delta(1232)$ in ref. [9]. The calculation of pion-nucleon scattering was extended up to $\mathcal{O}(q^4)$ in ref. [17], while isospin violation (including both strong isospin breaking terms and electromagnetism) is worked out up to $\mathcal{O}(q^3)$ in ref. [18]. The same authors also studied the influence of the Δ -isobar within the small ϵ -expansion [19] up to $\mathcal{O}(\epsilon^3)$ in ref. [20].^{#1} Isospin breaking corrections for the pion-nucleon scattering lengths to $\mathcal{O}(q^3)$ are calculated within IR in refs. [23, 24]. This is part of an on-going effort for providing high precision determinations of the pion-nucleon scattering lengths (a recent review on this issue is ref. [25]). Within IR CHPT πN scattering was already considered in refs. [26, 27]. Ref. [26] performed an $\mathcal{O}(q^4)$ one-loop calculation. Its main conclusion was that the one-loop representation is not precise enough to allow a sufficiently accurate extrapolation of physical data to the Cheng-Dashen point. On the other hand, ref. [27] was interested in the complementary aspects of comparing IR CHPT at $\mathcal{O}(q^3)$ to data and to previous HBCHPT studies [9, 16, 17]. The conclusions were unexpected and rather pessimistic. The description obtained was restricted to very low center-of-mass (CM) pion kinetic energy (less than 40 MeV), such that the IR results badly diverge from the experimental values above that energy in several partial waves [27]. In comparison, the resulting phase shifts in HBCHPT [9, 16] fit pion-nucleon phase shifts up to significantly higher energies and then start deviating smoothly from data. Last but not

^{#1}Other chiral power-countings including the explicit $\Delta(1232)$ resonance are the δ -expansion [21] and the more recent one of ref. [22].

least, ref. [27] also found an unrealistically large violation (20–30%) of the Goldberger-Treiman (GT) relation [28] for the pion-nucleon coupling. As we shall show, our results are somewhat more optimistic than those of ref. [27] because we obtain that IR is able to describe low-energy pion-nucleon scattering comparable to HBCHPT at $\mathcal{O}(q^3)$. Nevertheless, the caveat about the large violation of the GT relation in a full IR calculation at $\mathcal{O}(q^3)$ remains. When this calculation is restricted to strict $\mathcal{O}(q^3)$, as in HBCHPT, more realistic values around 2% are obtained for the violation of the GT relation.

As a consequence of unitarity, πN partial wave amplitudes develop a right-hand or unitarity cut with a branch point at the reaction threshold. The first derivative of the partial waves at this point is singular. Based on this, ref. [26] advocates for applying the chiral expansion to the subthreshold region of the πN scattering amplitude where it is expected to be smoother. This singularity can also be avoided by applying the chiral expansion to an interaction kernel which, by construction, has no right-hand cut. This is the so-called Unitary CHPT (UCHPT) [29, 30, 31, 32]. One of the consequences of this framework, is that the calculated πN partial waves fulfill unitarity. We compare in this work the purely perturbative results with those obtained by UCHPT, with the latter being able to fit data closely up to higher energies as shown below. There are other methods already employed to provide unitarized πN amplitudes from the given chiral expansions, e.g. [33, 34, 35]. We will also explore the region of the $\Delta(1232)$ resonance by including a Castillejo-Dalitz-Dyson (CDD) pole [36] in the inverse of the amplitude. The resulting amplitude has the same discontinuities along the right- and left-hand-cuts as the one without the CDD poles. Traditionally, this was a serious drawback for the bootstrap hypothesis [37, 38] since the source for dynamics in this approach is given precisely by the discontinuities of the amplitudes along the cuts. From our present knowledge based on QCD the presence of these extra solutions (including an arbitrary number of CDD poles) can be expected on intuitive grounds since they would be required in order to accommodate pre-existing resonances due to the elementary degrees of freedom of QCD. Alternatively, one could also include explicitly within the effective field theory the $\Delta(1232)$ resonances as a massive field [39, 40, 19, 27, 21, 22].

After this introduction we give in section 2 our conventions and Lagrangians employed, including kinematics and equations used to project into partial waves. The calculation at the one-loop level up to $\mathcal{O}(q^3)$ is performed in section 3, where we compare directly with the expressions given in ref. [26]. We also present fits to the experimental data at the perturbative level and discuss the resulting values for the chiral counterterms, scattering lengths and volumes and the violation of the GT relation. The resummation of the right-hand cut by means of UCHPT is undertaken in section 4, where we discuss the comparison with experimental data and the significant increase of the energy range for the reproduction of data. The conclusions are given in section 5.

2 Prelude: Generalities, kinematics and Lagrangians

We consider the process $\pi^a(q)N(p, \sigma; \alpha) \rightarrow \pi^{a'}(q')N(p', \sigma'; \alpha')$. Here a and a' denote the Cartesian coordinates in the isospin space of the initial and final pions with four-momentum q and q' , respectively. Regarding the nucleons, $\sigma(\sigma')$ and $\alpha(\alpha')$ correspond to the third-components of spin and isospin of the initial (final) states, in order. The usual Mandelstam variables are defined as $s = (p + q)^2 = (p' + q')^2$, $t = (q - q')^2 = (p - p')^2$ and $u = (p - q')^2 = (p' - q)^2$, that fulfill

$s + t + u = 2M_\pi^2 + 2m^2$ for on-shell scattering, with m and M_π the nucleon and pion mass, respectively. It is convenient to consider Lorentz- and isospin-invariant amplitudes (along our study exact isospin symmetry is presumed.) We then decompose the scattering amplitude as [41]

$$\begin{aligned} T_{aa'} &= \delta_{a'a} T^+ + \frac{1}{2} [\tau_a, \tau_{a'}] T^- , \\ T^\pm &= \bar{u}(p', \sigma') \left[A^\pm + \frac{1}{2} (\not{q}' + \not{q}'') B^\pm \right] u(p, \sigma) . \end{aligned} \quad (2.1)$$

Here, the Pauli matrices are indicated by τ_c . In the next section we will proceed with the calculation of A^\pm and B^\pm perturbatively up to $\mathcal{O}(q^3)$.

In IR the Feynman diagrams for πN scattering follow the standard chiral power counting [42]

$$\nu = 1 + 2L + \sum_i V_i (d_i + \frac{1}{2} n_i - 2) , \quad (2.2)$$

where L is the number of loops, V_i is the number of vertices of type i consisting of n_i baryon fields (in our case $n_i = 0, 2$) and d_i pion derivatives or masses. In this way, a given Feynman diagram for πN scattering counts as q^ν . For the calculation of pion-nucleon scattering up to $\mathcal{O}(q^3)$ we employ the chiral Lagrangian

$$\mathcal{L}_{CHPT} = \mathcal{L}_{\pi\pi}^{(2)} + \mathcal{L}_{\pi\pi}^{(4)} + \mathcal{L}_{\pi N}^{(1)} + \mathcal{L}_{\pi N}^{(2)} + \mathcal{L}_{\pi N}^{(3)} , \quad (2.3)$$

where the superscript indicates the chiral order, according to eq. (2.2). Here, $\mathcal{L}_{\pi\pi}^{(n)}$ refers to the purely mesonic Lagrangian without baryons and $\mathcal{L}_{\pi N}^{(n)}$ corresponds to the one bilinear in the baryon fields. We follow the same notation as in ref. [26] to make easier the comparison. Then,

$$\begin{aligned} \mathcal{L}_{\pi\pi}^{(2)} &= \frac{F^2}{4} \langle u_\mu u^\mu + \chi_+ \rangle , \\ \mathcal{L}_{\pi\pi}^{(4)} &= \frac{1}{16} \ell_4 (2 \langle u_\mu u^\mu \rangle \langle \chi_+ \rangle + \langle \chi_+ \rangle^2) + \dots \end{aligned} \quad (2.4)$$

where the ellipsis indicate terms that are not needed in the calculations given here. For the different symbols, F is the pion weak decay constant in the chiral limit and

$$u^2 = U , \quad u_\mu = iu^\dagger \partial_\mu U u^\dagger , \quad \chi_\pm = u^\dagger \chi u^\dagger \pm u \chi^\dagger u . \quad (2.5)$$

The explicit chiral symmetry breaking due to the non-vanishing quark masses (in the isospin limit $m_u = m_d = \hat{m}$) is introduced through $\chi = 2B_0 \hat{m}$. The constant B_0 is proportional to the quark condensate in the chiral limit $\langle 0 | \bar{q}^j q^i | 0 \rangle = -B_0 F^2 \delta^{ij}$. In the following we employ the so-called sigma-parameterization where

$$U(x) = \sqrt{1 - \frac{\vec{\pi}(x)^2}{F^2}} + i \frac{\vec{\pi}(x) \cdot \vec{\tau}}{F} \quad (2.6)$$

In eq. (2.4) we denote by $\langle \dots \rangle$ the trace of the resulting 2×2 matrix. For the pion-nucleon Lagrangian we have

$$\begin{aligned}
\mathcal{L}_{\pi N}^{(1)} &= \bar{\psi}(i \not{D} - \overset{\circ}{m})\psi + \frac{g}{2}\bar{\psi} \not{\psi} \gamma_5 \psi , \\
\mathcal{L}_{\pi N}^{(2)} &= c_1 \langle \chi_+ \rangle \bar{\psi} \psi - \frac{c_2}{4m^2} \langle u_\mu u_\nu \rangle (\bar{\psi} D^\mu D^\nu \psi + \text{h.c.}) + \frac{c_3}{2} \langle u_\mu u^\mu \rangle \bar{\psi} \psi - \frac{c_4}{4} \bar{\psi} \gamma^\mu \gamma^\nu [u_\mu, u_\nu] \psi + \dots , \\
\mathcal{L}_{\pi N}^{(3)} &= \bar{\psi} \left(-\frac{d_1 + d_2}{4m} ([u_\mu, [D_\nu, u^\mu]] + [D^\mu, u_\nu]) D^\nu + \text{h.c.}) \right. \\
&\quad + \frac{d_3}{12m^3} ([u_\mu, [D_\nu, u_\lambda]] (D^\mu D^\nu D^\lambda + \text{sym.}) + \text{h.c.}) + i \frac{d_5}{2m} ([\chi_-, u_\mu] D^\mu + \text{h.c.}) \\
&\quad + i \frac{d_{14} - d_{15}}{8m} (\sigma^{\mu\nu} \langle [D_\lambda, u_\mu] u_\nu - u_\mu [D_\nu, u_\lambda] \rangle D^\lambda + \text{h.c.}) \\
&\quad \left. + \frac{d_{16}}{2} \gamma^\mu \gamma_5 \langle \chi_+ \rangle u_\mu + \frac{id_{18}}{2} \gamma^\mu \gamma_5 [D_\mu, \chi_-] \right) \psi + \dots
\end{aligned} \tag{2.7}$$

In the previous equation $\overset{\circ}{m}$ is the nucleon mass in the chiral limit ($m_u = m_d = 0$) and the covariant derivative D_μ acting on the baryon fields is given by $\partial_\mu + \Gamma_\mu$ with $\Gamma_\mu = [u^\dagger, \partial_\mu u]/2$. The low-energy counterterms (LECs) c_i and d_i are not fixed by chiral symmetry and we fit them to πN scattering data. Again only the terms needed for the present study are shown in eq. (2.7). For more details on the definition and derivation of the different monomials we refer to refs. [16, 43].

The free one-particle states are normalized according to the Lorentz-invariant normalization

$$\langle \mathbf{p}', \sigma'; \gamma | \mathbf{p}, \sigma; \gamma \rangle = 2E_p (2\pi)^3 \delta(\mathbf{p}' - \mathbf{p}) \delta_{\sigma\sigma'} \delta_{\gamma\gamma'} , \tag{2.8}$$

where E_p is the energy of the particle with three-momentum \mathbf{p} and γ indicates any internal quantum number. A free two-particle state is normalized accordingly and it can be decomposed in states with well defined total spin S and total angular momentum J . For πN scattering $S = 1/2$ and one has in the CM frame

$$|\pi(-\mathbf{p}; a) N(\mathbf{p}, \sigma; \alpha)\rangle = \sqrt{4\pi} \sum_{\ell, m} (m\sigma\mu | \ell \frac{1}{2} J) Y_\ell^m(\hat{\mathbf{p}})^* |J\mu\ell; a\alpha\rangle , \tag{2.9}$$

with $\hat{\mathbf{p}}$ the unit vector of the CM nucleon three-momentum \mathbf{p} , ℓ the orbital angular momentum, m its third component and $\mu = m + \sigma$ the third-component of the total angular momentum. The Clebsch-Gordan coefficient is denoted by $(m_1 m_2 m_3 | j_1 j_2 j_3)$, corresponding to the composition of the spins j_1 and j_2 (with third-components m_1 and m_2 , in order) to give the third spin j_3 , with third-component m_3 . The state with total angular momentum well-defined, $|J\mu\ell; a\alpha\rangle$, satisfies the normalization condition

$$\langle J'\mu'\ell'; a'\alpha' | J\mu\ell; a\alpha \rangle = \delta_{JJ'} \delta_{\mu'\mu} \delta_{\ell\ell'} \frac{4\pi\sqrt{s}}{|\mathbf{p}|} \delta_{a'a} \delta_{\alpha'\alpha} . \tag{2.10}$$

The partial wave expansion of the πN scattering amplitude can be worked out straightforwardly from eq. (2.9). By definition, the initial baryon three-momentum \mathbf{p} gives the positive direction of

the \mathbf{z} -axis. Inserting the series of eq. (2.9) one has for the scattering amplitude

$$\langle \pi(-\mathbf{p}'; a') N(\mathbf{p}', \sigma'; \alpha') | T | \pi(-\mathbf{p}; a) N(\mathbf{p}, \sigma; \alpha) \rangle = 4\pi \sum_{\ell, m, J} Y_\ell^0(\hat{\mathbf{z}}) (m\sigma'\sigma | \ell \frac{1}{2} J) (0\sigma\sigma | \ell \frac{1}{2} J) Y_\ell^m(\hat{\mathbf{p}}') T_{J\ell}(s), \quad (2.11)$$

where T is the T-matrix operator and $T_{J\ell}$ is the partial wave amplitude with total angular momentum J and orbital angular momentum ℓ . Notice that in eq. (2.11) we made use of the fact that $Y_\ell^m(\hat{\mathbf{z}})$ is non-zero only for $m = 0$. Recall also that because of parity conservation partial wave amplitudes with different orbital angular momentum do not mix. From eq. (2.11) it is straightforward to isolate $T_{J\ell}$ with the result

$$T_{J\ell}(a', \alpha'; a, \alpha) = \frac{1}{\sqrt{4\pi(2\ell+1)}(0\sigma\sigma | \ell \frac{1}{2} J)} \sum_{m, \sigma'} \int d\hat{\mathbf{p}}' \langle \pi(-\mathbf{p}'; a') N(\mathbf{p}', \sigma'; \alpha') | T | \pi(-\mathbf{p}; a) N(\mathbf{p}, \sigma; \alpha) \rangle \times (m\sigma'\sigma | \ell \frac{1}{2} J) Y_\ell^m(\hat{\mathbf{p}}')^*. \quad (2.12)$$

In the previous expression the resulting $T_{J\ell}$ is of course independent of choice of σ .

The relation between the Cartesian and charge bases is given by

$$\begin{aligned} |\pi^+\rangle &= \frac{1}{\sqrt{2}}(|\pi^1\rangle + i|\pi^2\rangle), \\ |\pi^-\rangle &= \frac{1}{\sqrt{2}}(|\pi^1\rangle - i|\pi^2\rangle), \\ |\pi^0\rangle &= |\pi^3\rangle. \end{aligned} \quad (2.13)$$

According to the previous definition of states $|\pi^+\rangle = -|1, +1\rangle$, $|\pi^-\rangle = |1, -1\rangle$ and $|\pi^0\rangle = |\pi^3\rangle = |1, 0\rangle$, where the states of the isospin basis are placed to the right of the equal sign. Notice the minus sign in the relationship for $|\pi^+\rangle$. Then, the amplitudes with well-defined isospin, $I = 3/2$ or $1/2$, are denoted by $T_{IJ\ell}$ and can be obtained employing the appropriate linear combinations of $T_{J\ell}(a', \alpha'; a, \alpha)$, eq. (2.12), in terms of standard Clebsch-Gordan coefficients.

Due to the normalization of the states with well-defined total angular momentum, eq. (2.10), the partial waves resulting from eq. (2.12) with well defined isospin satisfy the unitarity relation

$$\text{Im}T_{IJ\ell} = \frac{|\mathbf{p}|}{8\pi\sqrt{s}} |T_{IJ\ell}|^2 \quad (2.14)$$

for $|\mathbf{p}| > 0$ and below the inelastic threshold due the one-pion production at $|\mathbf{p}| \simeq 210$ MeV. Given the previous equation, the S -matrix element with well defined I , J and ℓ , denoted by $S_{IJ\ell}$, corresponds to

$$S_{IJ\ell} = 1 + i \frac{|\mathbf{p}|}{4\pi\sqrt{s}} T_{IJ\ell}, \quad (2.15)$$

satisfying $S_{IJ\ell} S_{IJ\ell}^* = 1$ in the elastic physical region. In the same region we can then write

$$S_{IJ\ell} = e^{2i\delta_{IJ\ell}}, \quad (2.16)$$

with $\delta_{IJ\ell}$ the corresponding phase shifts.

3 Perturbative calculation and its results

From eq. (2.2) the leading order contribution to πN -scattering has $\nu = 1$ and it consists only of the lowest order pion-nucleon vertices with $d_i = 1$ and of no loops ($L = 0$). These diagrams correspond to the first two topologies shown from left to right in the first line of fig. 1, where all the diagrams up-to-and-including $\mathcal{O}(q^3)$ are shown. The $\mathcal{O}(q^2)$ or next-to-leading order (NLO) contribution still has no loops ($L = 0$) and contains an $\mathcal{O}(q^2)$ vertex with $d_i = 2$. It is shown by the third diagram in the first line of fig. 1. The NLO pion-nucleon vertex is depicted by the filled square. The $\mathcal{O}(q^3)$ or next-to-next-to-leading (N²LO) contributions consists of tree-level diagrams with at least one vertex of $d_i = 3$ type, with the other ones with $d_i = 1$. They are shown by the diagrams in the second line of fig. 1, where the diamond corresponds to the $d_i = 3$ vertex. Finally, at N²LO one also has the one loop ($L = 1$) diagrams involving only vertices with $d_i = 1$ from the LO pion-nucleon Lagrangian, $\mathcal{L}_{\pi N}^{(1)}$, and with $d_i = 2$ from the LO pure mesonic Lagrangian, $\mathcal{L}_{\pi\pi}^{(2)}$. The one-loop diagrams are the rest of those shown in the figure and are labelled with a latin letter (a)–(v). In addition, one also has the wave function renormalization of pions and nucleons affecting the LO contribution. The calculation is finally given in terms of m , F_π and g_A , which implies some reshuffling of pieces once the constants $\overset{\circ}{m}$, F and g in the chiral limit are expressed in terms of the physical m , F_π and g_A making use of their expressions at $\mathcal{O}(q^3)$ [26]. In this work we employ the numerical values $F_\pi = 92.4$ MeV, $M_\pi = 139$ MeV, $m_N = 939$ MeV, $g_A = 1.267$ and $\mu = m_N$.

The set of diagrams in fig. 1 was evaluated within IR CHPT in ref. [26] and we have re-evaluated it independently. We keep the same labelling for the one-loop diagrams as in this reference for easier comparison. We agree with all the one-loop integrals given in detail there. Regarding their contributions to A^\pm and B^\pm we also agree with all of them except for the contributions of the so-called integral $I_B^{(2)}$, that results from the tensor one-loop integrals with one meson and two baryon propagators, see appendix C of ref. [26]. We find that systematically all its contributions as given in ref. [26] should be reversed in sign. These contributions appear in diagrams (c)+(d), (g)+(h) and (i). Apart from the direct calculation, we have checked that the expressions given in ref. [26] violate perturbative unitarity. The latter results because unitarity, eq. (2.14), is a non-linear relation that mixes up orders in a power expansion. Denoting with a superscript the chiral order so that $T_{IJ\ell} = T_{IJ\ell}^{(1)} + T_{IJ\ell}^{(2)} + T_{IJ\ell}^{(3)} + \mathcal{O}(q^4)$ the unitarity relation eq. (2.14) up to $\mathcal{O}(q^3)$ implies

$$\text{Im}T_{IJ\ell}^{(3)} = \frac{|\mathbf{p}|}{8\pi\sqrt{s}} \left(T_{IJ\ell}^{(1)}\right)^2. \quad (3.1)$$

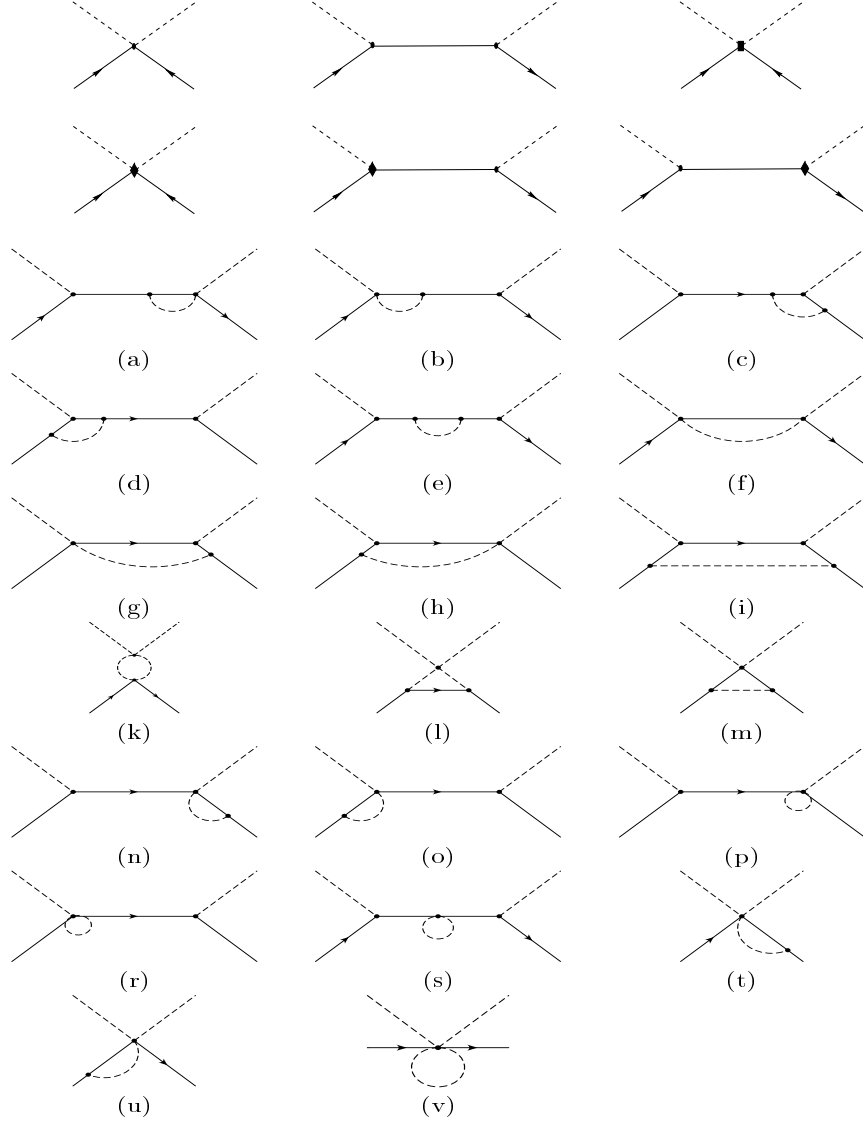


Figure 1: Set of diagrams for πN scattering up to-and-including $\mathcal{O}(q^3)$. The $\mathcal{O}(q)$ diagrams are the first two in the first line, from left to right. The $\mathcal{O}(q^2)$ contributions correspond to the third one still in the first line, where the $d_i = 2$, $n_2 = 2$ vertex is indicated with a square. The rest of the diagrams from the second line until the bottom of the figure are $\mathcal{O}(q^3)$. The $d_i = 3$, $n_i = 2$ vertices are indicated with a diamond. The one-loop diagrams only have lowest order pion-nucleon vertices.

Our expressions fulfill eq. (3.1), and those of ref. [26] also do once the sign in front of $I_B^{(2)}$ is reversed for all its contributions.^{#2} Technically we follow the general procedure of refs. [8] for calculating within IR and we do not give any expression for the different integrals calculated here because they were given already in refs. [44, 26, 8].

Now we proceed to compare our perturbative calculation with the experimental phase shifts

^{#2}The authors of ref. [26] state in page 30 that the scattering amplitude calculated obeys perturbative unitarity. It seems then that the difference in the sign referred above corresponds to a typo of [26].

for the low-energy data on the πN S - and P -waves (which are the relevant partial waves for such energies.) Since our solution is perturbative one should evaluate the phase shifts in a chiral expansion too. From the relation between $S_{IJ\ell}$ and $T_{IJ\ell}$, eq. (2.15), one has

$$T_{IJ\ell} = \frac{8\pi\sqrt{s}}{|\mathbf{p}|} \sin \delta_{IJ\ell} e^{i\delta_{IJ\ell}} ,$$

$$\cos \delta_{IJ\ell} \sin \delta_{IJ\ell} = \frac{|\mathbf{p}|}{8\pi\sqrt{s}} \text{Re}T_{IJ\ell} . \quad (3.2)$$

Which implies that δ starts at $\mathcal{O}(q^2)$ so that up to $\mathcal{O}(q^4)$ one can write

$$\delta_{IJ\ell} = \frac{|\mathbf{p}|}{8\pi\sqrt{s}} \text{Re}T_{IJ\ell} , \quad (3.3)$$

with $T_{IJ\ell}$ evaluated in the IR CHPT series (in our present case up to $\mathcal{O}(q^3)$.)

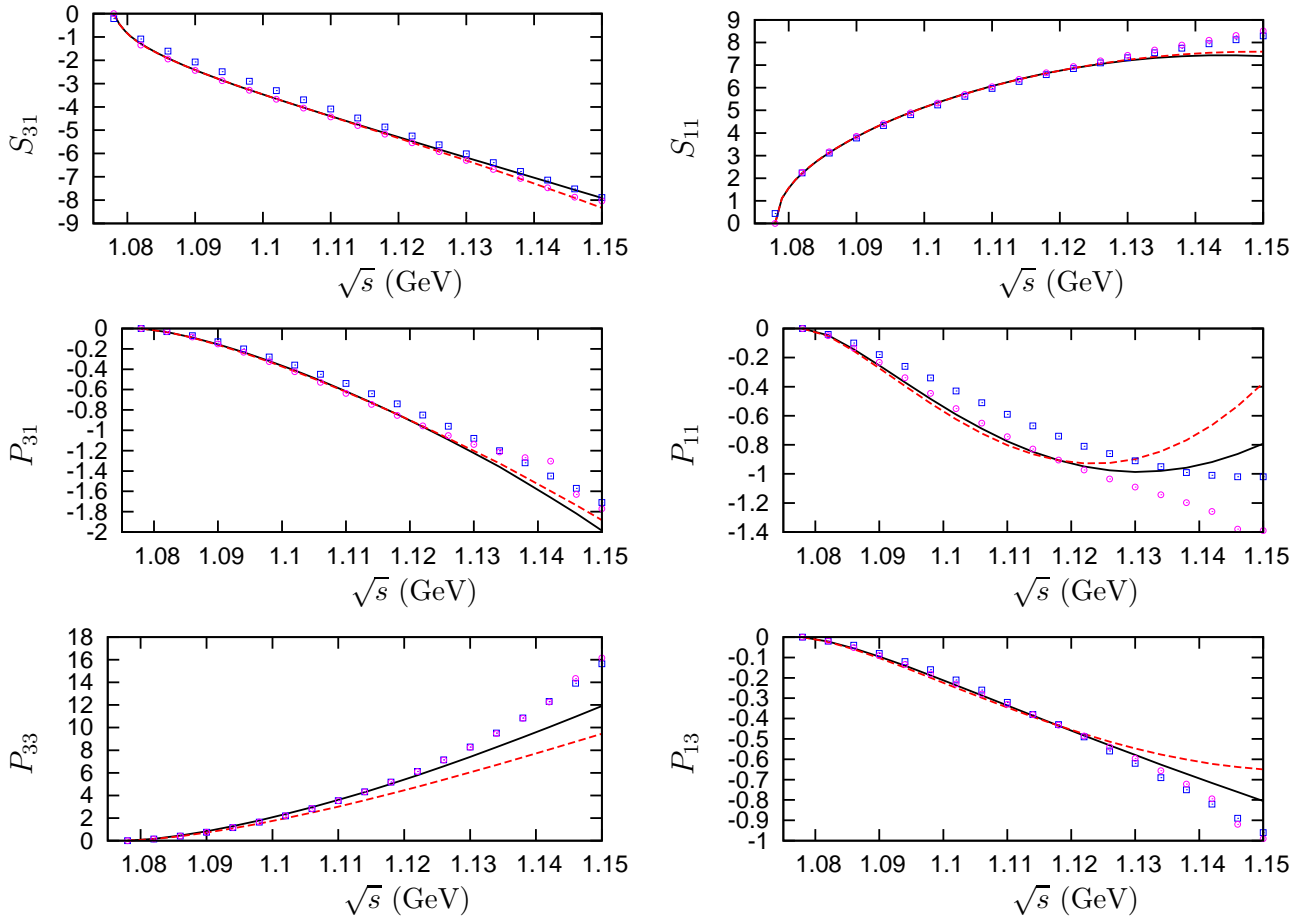


Figure 2: (Color online.) Fits to the KA85 pion-nucleon phase shifts [45] as a function of \sqrt{s} (in GeV) for $\sqrt{s}_{max} = 1.13$ GeV in IR CHPT at $\mathcal{O}(q^3)$. The KA85-1 fit corresponds to the solid curves and the KA85-2 fit to the dashed ones. Data points: circles are KA85 and squares WI08 data.

We now consider the reproduction of the πN phase shifts of the partial wave analyses of the Karlsruhe (KA85) group [45] and the current one of the GWU (WI08) group [46]. The fits are done with the full IR CHPT calculation to $\mathcal{O}(q^3)$. Due to the absence of error in these analyses [45, 46] there is some ambiguity in the definition of the χ^2 . Here we follow a similar strategy to that of ref. [31] and define an error assigned to every point as the sum in quadrature of a systematic plus a statistical error,

$$\text{err}(\delta) = \sqrt{e_s^2 + e_r^2 \delta^2}, \quad (3.4)$$

where e_s is the systematic error and e_r the relative one. In ref. [16] a relative error of 3% was taken while in ref. [31] a 5% error was considered. In the following we take for e_s just 0.1 degrees and $e_r = 2\%$. Regarding these values for the errors notice that isospin breaking corrections in πN scattering are estimated to be rather small (ref. [47] estimates for S -waves an isospin breaking correction $\lesssim 1\%$.) We then consider the larger 2% value as a safer estimate for isospin breaking effects not taken into account in our isospin symmetric study. Notice also that the $\mathcal{O}(q^4)$ contributions are expected to be suppressed compared with the leading term by a relative factor $\sim (M_\pi/\Lambda)^3 \sim (0.14/0.5)^3 \sim 0.02$. Although small, a finite value for e_s helps to stabilize fits. Otherwise, with $e_s = 0$, extra weight is given to the small energy region close to threshold, where the phase shifts are smaller and absolute errors decrease. Tiny differences between the calculation and points in the input become then exceedingly relevant. We take $e_s = 0.1$ degrees since it is much smaller than typical values of the phase shifts and is also the typical size for the difference between the phase shifts of refs. [45, 46] in the low-energy region for the P_{11} partial wave (compare the squares [45] and the circles [46] in fig. 2.) We have also convinced ourselves that changes in these values for e_s and e_r do not affect our conclusions.

The χ^2 function to be minimized is defined in a standard way as

$$\chi^2 = \sum_i \frac{(\delta - \delta_{th})^2}{\text{err}(\delta)^2}, \quad (3.5)$$

with δ_{th} the phase shift calculated theoretically. For the minimization process we employ the program MINUIT [48].

First, we discuss the reproduction of the KA85 data [45] and later the WI08 [46] ones. As a first strategy, we fit directly these data from threshold up to an upper value denoted by \sqrt{s}_{max} , and consider several values for \sqrt{s}_{max} . A data point is included every 4 MeV in \sqrt{s} . One observes that the χ^2 per degree of freedom ($\chi_{d.o.f.}^2$) is below 1 for $\sqrt{s}_{max} \lesssim 1.13$ GeV, and then rises fast with energy so that for $\sqrt{s}_{max} = 1.14$ GeV the $\chi_{d.o.f.}^2$ is 2.1 and for $\sqrt{s}_{max} = 1.15$ GeV it becomes 3.6. In fig. 2 we show by the solid line the result of the fit for $\sqrt{s}_{max} = 1.13$ GeV. At the level of the resulting curves the differences are small when varying \sqrt{s}_{max} within the range indicated above. A good reproduction of the data is achieved up to around $\sqrt{s} \lesssim 1.14$ GeV, a similar range of energies to that obtained in the $\mathcal{O}(q^3)$ HBCHPT fits of Fettes and Meißner [16]. From fig. 2 one can readily see the origin of the rise in the χ^2 with increasing \sqrt{s}_{max} . It stems from the last points of the partial waves P_{33} , P_{31} and P_{11} for which the resulting curves depart from them, getting worse as the energy increases. The fast rising of the P_{33} phase shifts is due to the $\Delta(1232)$ resonance. Though the tail of this resonance is mimicked in CHPT by the LECs, its energy dependence is too steep to be completely accounted for at $\mathcal{O}(q^3)$ due to the closeness of

LEC	KA85-1	KA85-2	HBCHPT $\mathcal{O}(q^3)$ [16]	HBCHPT Disp. [49]	HBCHPT $\mathcal{O}(q^3)$ [50]	RS [50]
c_1	-0.71 ± 0.49	-0.79 ± 0.51	$(-1.71, -1.07)$	-0.81 ± 0.12	-1.02 ± 0.06	
c_2	4.32 ± 0.27	3.49 ± 0.25	$(3.0, 3.5)$	8.43 ± 56.9	3.32 ± 0.03	3.9
c_3	-6.53 ± 0.33	-5.40 ± 0.13	$(-6.3, -5.8)$	-4.70 ± 1.16	-5.57 ± 0.05	-5.3
c_4	3.87 ± 0.15	3.32 ± 0.13	$(3.4, 3.6)$	3.40 ± 0.04		3.7
$d_1 + d_2$	2.48 ± 0.59	0.94 ± 0.56	$(3.2, 4.1)$			
d_3	-2.68 ± 1.02	-1.10 ± 1.16	$(-4.3, -2.6)$			
d_5	2.69 ± 2.20	1.86 ± 2.28	$(-1.1, 0.4)$			
$d_{14} - d_{15}$	-1.71 ± 0.73	1.03 ± 0.71	$(-5.1, -4.3)$			
d_{18}	-0.26 ± 0.40	-0.07 ± 0.44	$(-1.6, -0.5)$			

Table 1: Columns 2–5: Values of the low-energy constants for the KA85-1 and KA85-2 fits. The c_i are given in GeV^{-1} and the d_i (or their combinations) in GeV^{-2} . The renormalization scale for $d_i(\lambda)$ is $\lambda = 1 \text{ GeV}$. The interval of values obtained in [16] by fitting low-energy πN scattering data with HBCHPT at $\mathcal{O}(q^3)$ is given in the fourth column. Other determinations are given in columns fifth [49] and sixth [50]. Resonance saturation estimates are collected in the last column [50].

the $\Delta(1232)$ to the πN threshold. Indeed, this deficiency already occurred in the $\mathcal{O}(q^3)$ HBCHPT calculation of ref. [16]. However, at $\mathcal{O}(q^4)$ the fit to data improves because of the appearance of new higher order LECs [17].

The resulting values for the CHPT LECs are shown in the second column of table 1, denoted by KA85-1, in units of GeV^{-1} and GeV^{-2} for the c_i and d_i , respectively. Note that at $\mathcal{O}(q^3)$ only the combinations of counterterms $d_1 + d_2$, d_3 , d_5 , $d_{14} - d_{15}$ and d_{18} appear in πN scattering. The first four combinations were already explicitly shown in the expression for $\mathcal{L}_{\pi N}^{(3)}$, eq. (2.7). The counterterm d_{16} does not appear because it is re-absorbed in the physical value of the pion-nucleon axial-vector coupling g_A , once the lowest order g constant is fixed in terms of the former [26]. Under variations of $\sqrt{s_{max}}$ most of the counterterms present a rather stable behavior, with the $\mathcal{O}(q^3)$ ones being the most sensitive. The change in the LECs when varying $\sqrt{s_{max}}$ between 1.12 to 1.15 GeV is a source of uncertainty that is added in quadrature with the statistical error from the fit with $\sqrt{s_{max}} = 1.13 \text{ GeV}$, which has a $\chi_{d.o.f.}^2$ of 0.9. The central values shown correspond to the same fit too. We also show in the table the values obtained from other approaches at $\mathcal{O}(q^3)$ [50, 15, 16, 49], including the $\mathcal{O}(q^3)$ HBCHPT fit to πN data [16], the dispersive analysis within the Mandelstam triangle of ref. [49] and the results at $\mathcal{O}(q^3)$ from ref. [50], that also includes an estimation of the $\mathcal{O}(q^2)$ LECs from resonance saturation (RS). Within uncertainties, our values for c_1 , c_3 and c_4 are compatible with these other determinations. Instead, c_2 is somewhat larger, which is one of the main motivations for considering other fits to πN scattering following the so called strategy 2, as explained below. Our values are also compatible with those determined from the πN parameters up to $\mathcal{O}(q^4)$ in ref. [51] that gives the intervals $c_1 = (-1.2, -0.9)$, $c_2 = (2.6, 4.0)$ and $c_3 = (-6.1, -4.4)$. The threshold parameters taken in this analysis are those calculated in ref. [45]. Regarding the $\mathcal{O}(q^3)$ counterterms the comparison with HBCHPT is not so clear due to the large uncertainties both from our side as well as from [16]. As discussed in more detail below, the $\mathcal{O}(q^3)$ contribution is typically the smallest between the different orders studied so

that it is harder to pin down precise values for these counterterms. Indeed, we observe from the second column in table 1 that d_3 , d_5 and $d_{14} - d_{15}$ have large errors, much larger than those of the $\mathcal{O}(q^2)$ counterterms (although the error estimated for c_1 is also large because the fits are not very sensitive to this counterterm which is multiplied by the small M_π^2 without energy dependence.) Our values for the LECs d_i , again within the large uncertainties, are compatible with those of ref. [16]. Only $d_{14} - d_{15}$ is larger in our case, out of the range given in [16] by around a factor 2.

The threshold parameters for the fit KA85-1 are collected in the second column of table 2. We have evaluated the different scattering lengths and volumes by performing an effective range expansion (ERE) fit to our results in the low-energy region (namely, for $|\mathbf{p}| < M_\pi^2(1 - M_\pi^2/m^2)$ which sets the range of the ERE.)^{#3} The error given to our threshold parameters is just statistical. It is so small because the values of the scattering lengths and volumes are rather stable under changes of \sqrt{s}_{max} and LECs within their uncertainties (taking into account the correlation among them.) If treated in an uncorrelated way the error would be much larger. We also vary the numbers of terms in the ERE expansion from 3 to 5 and the slight variation in the resulting scattering lengths/volumes is also taken into account in the errors given. In the last two columns of table 2, we give the values from the partial wave analyses of refs. [45, 46]. Notice that the differences between the central values from the latter two references are larger than one standard deviation, except for the P_{33} case. The differences between the S_{31} scattering lengths and P_{13} scattering volumes are specially large. Given this situation we consider that our calculated scattering lengths and volumes are consistent with the values obtained in the KA85 and WI08 partial wave analyses, except for the P_{33} one for which our result is significantly larger. It is also too large compared with the values obtained in the $\mathcal{O}(q^3)$ HBCHPT fits to phase-shifts of ref. [16].

Partial Wave	KA85-1	KA85-2	KA85	WI08
$a_{S_{31}}$	-0.100 ± 0.001	-0.103 ± 0.001	-0.100 ± 0.004	-0.084
$a_{S_{11}}$	0.171 ± 0.001	0.172 ± 0.002	0.175 ± 0.003	0.171
a_{0+}^+	-0.010 ± 0.001	-0.011 ± 0.001	-0.008^a	-0.0010 ± 0.0012
a_{0+}^-	0.090 ± 0.001	0.092 ± 0.001	0.092^a	0.0883 ± 0.0005
$a_{P_{31}}$	-0.052 ± 0.001	-0.051 ± 0.001	-0.044 ± 0.002	-0.038
$a_{P_{11}}$	-0.078 ± 0.001	-0.088 ± 0.001	-0.078 ± 0.002	-0.058
$a_{P_{33}}$	0.251 ± 0.002	0.214 ± 0.002	0.214 ± 0.002	0.194
$a_{P_{13}}$	-0.034 ± 0.001	-0.035 ± 0.001	-0.030 ± 0.002	-0.023

Table 2: S -wave scattering lengths and P -wave scattering volumes in units of M_π^{-1} and M_π^{-3} , respectively. Our results for the fits to the KA85-1 and KA85-2 are given in the second and third columns, respectively. The fourth column corresponds to the values of the KA85 analysis [45]. The values for WI08 are extracted from ref. [46] and the errors, when given, from ref. [52].

^a These numbers are given without errors because no errors are provided in ref. [45]. They are deduced from the KA85 ones for $a_{S_{31}}$ and $a_{S_{11}}$.

^{#3}Numerical problems arising for $|\mathbf{p}| \rightarrow 0$ prevent to calculate directly the threshold parameters as $\lim_{\mathbf{p} \rightarrow 0} |\mathbf{p}| \text{Re } T / 8\pi\sqrt{s} |\mathbf{p}|^{1+2L}$.

Due to the large values for c_2 and $a_{P_{33}}$ we consider that the fit KA85-1 is not completely satisfactory and try a second strategy (KA85-2). As it was commented above, the rapid increase in the phase shifts due to the tail of the $\Delta(1232)$ is not well reproduced at $\mathcal{O}(q^3)$. As a result, instead of fitting the P_{33} phase shifts as a function of energy we fit now the function $\tan \delta_{P_{33}}/|\mathbf{p}|^3$ for three points with energy less than 1.09 GeV, where $\delta_{P_{33}}$ is the phase shifts for the P_{33} partial wave. The form of this function is, of course, dictated by the ERE and at threshold it directly gives the corresponding scattering volume. We take a 2% of error for these points because within errors this is the range of values spanned in table 2 by the KA85 and WI08 results for $a_{P_{33}}$. A relative error of 2% was also taken for e_r in eq. (3.4). The resulting values for the LECs are given in the third column of Table 1 and the curves for $\sqrt{s}_{max} = 1.13$ GeV are shown in fig. 2 by the dashed lines, that have a $\chi^2_{d.o.f.} = 0.86$. We observe that these curves are quite similar to the ones previously obtained in KA85-1. Nevertheless, for the P_{11} partial wave the description is slightly worse above 1.12 GeV and it is the main contribution to the final χ^2 . For the P_{33} phase shifts one also observes a clear difference between the two curves as the dashed line runs lower than the solid line. The former reproduces the standard values for the P_{33} scattering volume, see column three of Table 2, while for the latter it is larger. This is another confirmation that the description of the rapid rise of the P_{33} phase shifts at $\mathcal{O}(q^3)$ enforces the fit to enlarge the value of the resulting scattering volume. It is remarkable that now the value of the $\mathcal{O}(q^2)$ LEC c_2 is smaller and perfectly compatible with the interval of values of [16]. It is also interesting to note that c_3 is also smaller, which is a welcome feature especially for two- and few-nucleon systems that are rather sensitive to large sub-leading two-pion exchange NN potential that is generated by the inclusion of the c_1 , c_3 and c_4 [53]. See refs. [54, 55, 56] for a thorough discussion on this issue for two- and few-nucleon systems. Related to this point, one has determinations of c_3 and c_4 by a partial wave analysis of the pp and np scattering data from ref. [57] with the results

$$\begin{aligned} c_3 &= -4.78 \pm 0.10 \text{ GeV}^{-1} , \\ c_4 &= +3.96 \pm 0.22 \text{ GeV}^{-1} . \end{aligned} \tag{3.6}$$

The systematic errors are not properly accounted for yet in these determinations due to the dependence on the matching point that distinguishes between the long-range part of the NN potential (parameterized from CHPT) and the short-range one (with a purely phenomenological parameterization.) Namely, the same authors in ref. [58] considered this issue and when varying the matching point from 1.8 fm to 1.4 fm the LECs changed significantly: $c_3 = -5.08(28) \rightarrow -4.99(21)$ and $c_4 = 4.70(70) \rightarrow 5.62(69) \text{ GeV}^{-1}$. With respect to the $\mathcal{O}(q^3)$ counterterms we see that the central values have shifted considerably compared with KA85-1. This clearly indicates that these LECs cannot be properly pinned down by fitting πN scattering data. Within uncertainties d_3 , d_5 and d_{18} overlap at the level of one sigma. The LECs $d_1 + d_2$ and $d_{14} - d_{15}$ require to take into account a variation of 2 sigmas. In view of this situation we consider that one should be conservative and give ranges of values for these latter combination of LECs in order to make them compatible

$$\begin{aligned} d_1 + d_2 &= +0.4 \dots + 3 \text{ GeV}^{-2} , \\ d_{14} - d_{15} &= -2.4 \dots + 1.75 \text{ GeV}^{-2} . \end{aligned} \tag{3.7}$$

These values correspond to the minimum and maximum of those shown in the second and third columns of table 1 allowing a variation of one sigma.

The scattering lengths and volumes for KA85-2 are collected in the third column of Table 2. They are calculated from our results similarly as explained above for the KA85-1 fit. It is remarkable that now the value for the P_{33} scattering volume is perfectly compatible with the determinations from KA85 and WI08. We see a good agreement between our $\mathcal{O}(q^3)$ IR CHPT results and the scattering lengths/volumes for KA85. Only the P_{11} scattering volume is slightly different, though the difference between the KA85 and WI08 results is significantly large for this case too. One also observes differences beyond the error estimated in KA85 for the P_{13} scattering volume between the KA85 and WI08 values. Ours is closer to the KA85 one.

It is also worth emphasizing that our fits to the phase shifts of the KA85 analysis (KA85-1 and KA85-2), as shown in fig. 2, offer a good reproduction of the data and the worsening for higher energies stems in a smooth way as in $\mathcal{O}(q^3)$ HBCHPT [16]. This is certainly an improvement compared with the previous πN study in IR CHPT to $\mathcal{O}(q^3)$ of ref. [27]. In this latter reference, data could only be fitted up to around 1.12 GeV and large discrepancies above that energy, rapidly increasing with energy, emerged in the S_{31} , P_{13} and P_{11} partial waves.

We proceed along similar lines and perform fits of type 1 and 2 to the current solution of the GWU group [46] (WI08). These fits are denoted by WI08-1 and WI08-2, in that order. The resulting curves for $\sqrt{s}_{max} = 1.13$ GeV are shown by the solid and dashed lines in fig. 3, respectively. One observes very similar curves to the KA85-1 and KA85-2 fits except for the P_{11} phase shifts. Here, the agreement with the WI08 data is considerably worse. This has a clear translation into the values of the χ^2 for this partial wave, which increases almost by a factor 3, from 20 (KA85-2) to 55 (WI08-2) (the number of fitted points is 12.) It is clear from fig. 3 that IR CHPT at $\mathcal{O}(q^3)$ does not compare well with the P_{11} WI08 phase shifts even at very low energies, $\sqrt{s} < 1.11$ GeV. For the KA85 data the situation is much better, compare with fig. 2. Indeed, previous solutions of the GWU (and prior VPI) group had a behavior similar to that of KA85 for the P_{11} phase-shifts, e.g. the solution SM01 employed in the analysis of ref. [27] also using IR CHPT at $\mathcal{O}(q^3)$. In view of the difficulties of our study based on IR CHPT at $\mathcal{O}(q^3)$ for reproducing the P_{11} phase shifts of WI08 at low energies we consider advisable a revision of the current solution WI08 of the GWU group and the way the ηN data affect the low-energy P_{11} phase shifts in the coupled channel approach followed [59].

The other distinctive features when comparing strategies 1 and 2 for the fits to the WI08 data are similar to those already discussed for the KA85 fits. In this way, one has for WI08-1 that c_2 and c_3 have a value in modulus larger by around 1 GeV⁻¹ than for WI08-2. Related to this, the P_{33} scattering volume is also significantly larger for WI08-1 than for WI08-2. The values of the fitted LECs for WI08-1 and WI08-2 are collected in the second and third columns of Table 3. One observes that the resulting LECs at $\mathcal{O}(q^2)$ are quite similar between KA85-1, WI08-1, on the one hand, and KA85-2, WI08-2, on the other, so that within uncertainties they are compatible in either of the two strategies. In the third column of Table 3 we present the average of the LECs from our fits in Tables 1 and 3. The error given for every LEC is the sum in quadrature of the largest of the statistical errors shown in the previous tables and the one resulting from the dispersion in the central values. This is a conservative procedure which recognizes that both strategies are acceptable for studying low-energy πN scattering and that takes into account the

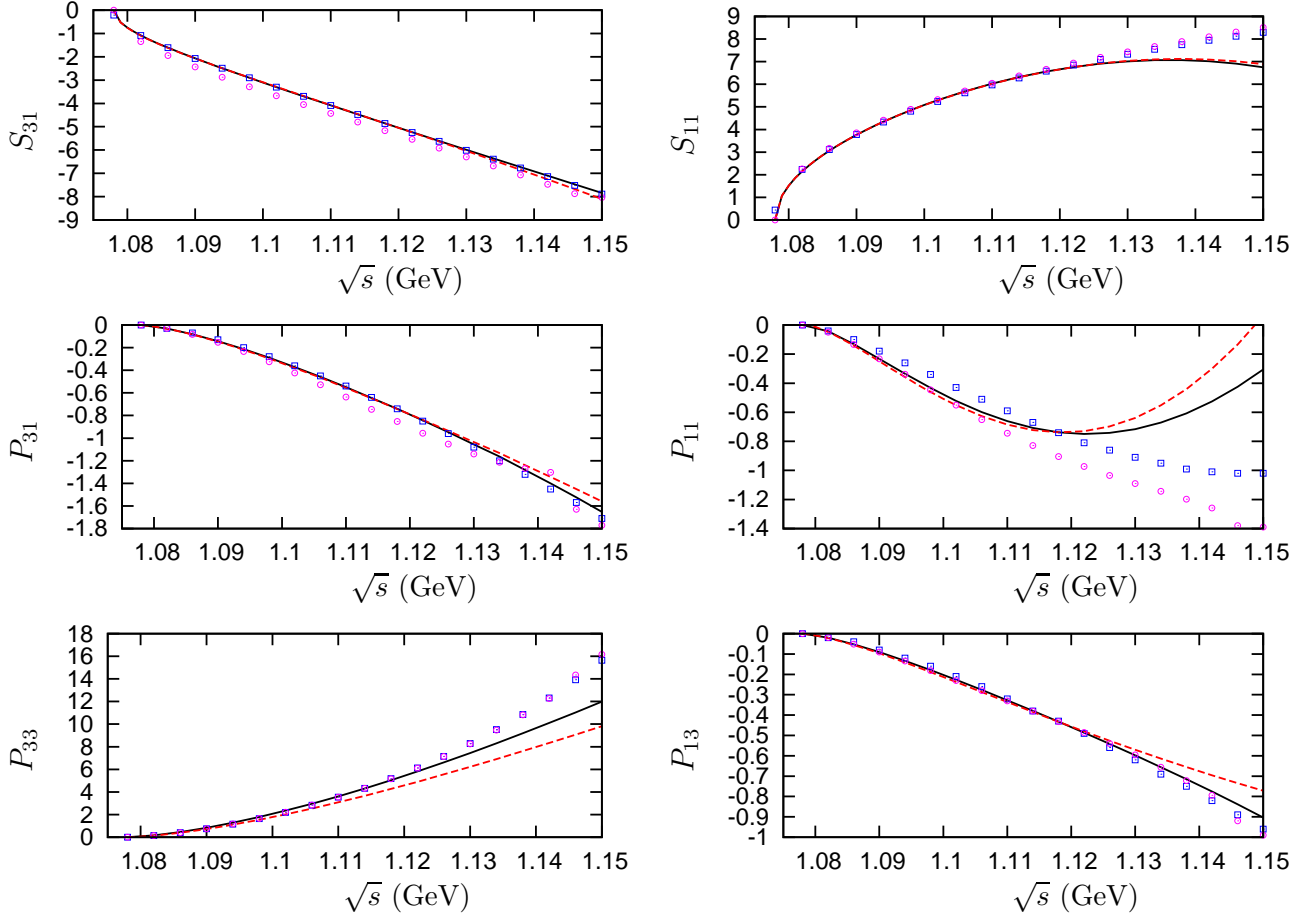


Figure 3: (Color online.) Fits to the WI08 pion-nucleon phase shifts [46] as a function of \sqrt{s} (in GeV) for $\sqrt{s}_{max} = 1.13$ GeV in IR CHPT at $\mathcal{O}(q^3)$. The WI08-1 fit corresponds to the solid curves and the WI08-2 fit to the dashed ones. Data points: circles are KA85 and squares WI08 data.

dispersion in the LECs that results from changes in the data set. Within errors, the values of the LECs in the last column of Table 3 are compatible with those from HBCHPT at $\mathcal{O}(q^3)$ ($d_{14} - d_{15}$ is the only counterterm that differs by more than one standard deviation from the interval of values of ref. [16].)

Regarding the threshold parameters we list in the second and third columns of Table 4 the values for the S -wave scattering lengths and P -wave scattering volumes corresponding to the fits WI08-1 and WI08-2 with $\sqrt{s}_{max} = 1.13$ GeV (the same fits shown in fig. 3.) The procedure for their determination is the same as the one already discussed for KA85-1. The largest changes compared with the values of the KA85-1 and KA85-2 fits, respectively, occur for the $a_{S_{31}}$ and $a_{P_{11}}$ scattering length and volume, in order. The latter also shows the largest difference between the results of the fits following strategy 1 and 2 (a 12% of relative difference for the KA85 case and a 9% for the WI08 one.) Nonetheless, neither of our results for $a_{P_{11}}$, including strategy 1 and 2 KA85 and WI08 fits, is compatible with the value of WI08 [46], shown in the last column of Table 2. The largest difference occurs for the value of KA85-2 which is a 50% smaller than the one from

WI08. Coming back to the WI08 fits, we note that the isoscalar S -wave scattering length a_{0+}^+ is now a vanishing positive number while the P_{11} scattering volume has decreased, and is compatible with the KA85 result within one sigma. We notice that the tiny errors estimated for the threshold parameters resulting from our fits in Tables 2 and 4 are just statistical and are determined in the same way as explained above for the KA85-1 fit. Of course, systematic errors due to higher orders in the chiral expansion and different data sets taken induce larger systematic uncertainties than the small errors shown. In this sense, the difference between the values obtained for each partial wave in these columns provides a better estimation of uncertainties. We then calculate the average^{#4} of the four values for each scattering length/volume shown altogether in Tables 2 and 4. This is given in the last column of Table 4. We also see that our averaged values for the a_{0+}^+ and a_{0+}^- scattering lengths are compatible with the results obtained in ref. [60], $a_{0+}^+ = 0.0015 \pm 0.0022$ and $a_{0+}^- = 0.0852 \pm 0.0018 M_\pi^{-1}$, that takes into account isospin breaking corrections in the analysis of recent experimental results on pionic hydrogen and pionic deuterium data

LEC	WI08-1	WI08-2	Average
c_1	-0.27 ± 0.51	-0.30 ± 0.48	-0.52 ± 0.60
c_2	4.28 ± 0.27	3.55 ± 0.30	3.91 ± 0.54
c_3	-6.76 ± 0.27	-5.77 ± 0.29	-6.12 ± 0.72
c_4	4.08 ± 0.13	3.60 ± 0.16	3.72 ± 0.37
$d_1 + d_2$	2.53 ± 0.60	1.16 ± 0.65	1.78 ± 1.1
d_3	-3.65 ± 1.01	-2.32 ± 1.04	-2.44 ± 1.6
d_5	5.38 ± 2.40	4.83 ± 2.18	3.69 ± 2.93
$d_{14} - d_{15}$	-1.17 ± 1.00	1.27 ± 1.11	-0.145 ± 1.88
d_{18}	-0.86 ± 0.43	-0.72 ± 0.40	-0.48 ± 0.58

Table 3: Fitted LECs in units of GeV^{-1} (c_i) and GeV^{-2} (d_i) for the fits WI08-1 and WI08-2 with $\sqrt{s}_{max} = 1.13$ GeV. The last columns is the average of all the fits in Tables 1 and 3.

Finally, we show in fig. 4 the different chiral order contributions to the total phase shifts (depicted by the solid lines) for the fit KA85-1 (shown in fig. 2 by the solid lines.) The dotted lines correspond to the leading result, the dashed ones to NLO and the dash-dotted ones to N²LO. A general trend observed is the partial cancellation between the $\mathcal{O}(q^2)$ and $\mathcal{O}(q^3)$ contributions. For the P -waves, the cancellation is almost exact at low energies while at higher energies the $\mathcal{O}(q^2)$ contribution is larger in modulus than the $\mathcal{O}(q^3)$ one (except for the P_{31} partial wave where the cancellation is almost exact all over the energy range shown, so that the first order describes well this partial wave.) For the S -waves at low energies ($\sqrt{s} \lesssim 1.11$ GeV) the first order contributions dominates, though the second order one tends to increase rapidly with energy. For these partial waves the second order contribution is much larger than the third order one and the partial cancellation between these orders is weak (even both orders add with the same sign for S_{31} at the highest energies shown.) The smallness of the third order contribution for the S -waves together with the fact that it is also clearly smaller than the second order one for most of the

^{#4}Not the weighted average. The given errors are calculated by adding in quadrature for each LEC the largest of the errors in Tables 1 and 3 and the one resulting from the average of values.

Partial Wave	WI08-1	WI08-2	Average
$a_{S_{31}}$	-0.081 ± 0.001	-0.082 ± 0.001	-0.092 ± 0.012
$a_{S_{11}}$	0.165 ± 0.002	0.167 ± 0.002	0.169 ± 0.004
a_{0+}^+	0.001 ± 0.001	0.001 ± 0.001	-0.005 ± 0.007
a_{0+}^-	0.082 ± 0.001	0.083 ± 0.001	0.087 ± 0.005
$a_{P_{31}}$	-0.048 ± 0.001	-0.051 ± 0.001	-0.051 ± 0.002
$a_{P_{11}}$	-0.073 ± 0.001	-0.080 ± 0.001	-0.080 ± 0.006
$a_{P_{33}}$	0.252 ± 0.002	0.222 ± 0.002	0.232 ± 0.017
$a_{P_{13}}$	-0.032 ± 0.001	-0.035 ± 0.001	-0.034 ± 0.002

Table 4: S -wave scattering lengths and P -wave scattering volumes in units of M_π^{-1} and M_π^{-3} , respectively, for the fits WI08-1 and WI08-2 with $\sqrt{s}_{max} = 1.13$ GeV. The last column corresponds to the averaged values of the threshold parameters of all the fits in Tables 2 and 4.

P -waves explain the difficulties to pin down precise values for the $\mathcal{O}(q^3)$ LECs (the d_i 's), as already indicated above.

The LEC d_{18} is important as it is directly involved in the violation of the GT relation [28]. Up to $\mathcal{O}(M_\pi^3)$ one has [16, 26]

$$g_{\pi N} = \frac{g_A m}{F_\pi} \left(1 - \frac{2M_\pi^2 d_{18}}{g_A} \right). \quad (3.8)$$

We quantify the deviation from the GT relation by

$$\Delta_{GT} = \frac{g_{\pi N} F_\pi}{g_A m} - 1. \quad (3.9)$$

Inserting our averaged value of d_{18} in the third column of Table 3 into eq. (3.8), we then find

$$\Delta_{GT} = 0.015 \pm 0.018, \quad (3.10)$$

which is compatible with the values around 2–3% that are nowadays preferred from πN and NN partial wave analyses [61, 62, 63]. In terms of the πN coupling constant, from eq. (3.8) our value for d_{18} translates in

$$g_{\pi N} = 13.07 \pm 0.23 \quad (3.11)$$

or $f^2 = (g_{\pi N} M_\pi / 4m)^2 / \pi = 0.077 \pm 0.003$. Within uncertainties our result at strict $\mathcal{O}(M_\pi^3)$ is compatible at the level of one sigma with the determinations of refs. [61, 62, 63].

However, IR CHPT at $\mathcal{O}(q^3)$ gives rise to a caveat concerning the GT relation. The point is that the full calculation at this order (IR CHPT contains higher orders due to the $1/m$ relativistic resummation) produces a huge GT relation violation of about a 20%, similarly as in ref. [27]. For the evaluation of the GT relation discrepancy in our present calculations we study the $\pi^- p \rightarrow \pi^- p$ scattering. We select this particular process in the charge basis of states because the crossed u -channel process, $\pi^+ p \rightarrow \pi^+ p$, is purely $I = 3/2$ and thus there is no u -channel nucleon pole, which

requires the same quantum numbers as for the nucleon, in the isospin limit. Otherwise the s - and u -channel nucleon poles overlap for some values of the scattering angle. When projecting the u -channel nucleon pole in a partial wave it produces a cut for $m^2 - 2M_\pi^2 + M_\pi^4/m^2 < s < m^2 + 2M_\pi^2$, with the branch points very close to the nucleon pole at $s = m^2$. As a result, there is not soft way to calculate the residue at the s -channel nucleon pole unless the u -channel nucleon pole is removed, as done by considering the $\pi^- p \rightarrow \pi^- p$ scattering. The latter is finally projected in the partial wave P_{11} , with the same quantum numbers as the nucleon. The ratio of the residues at the nucleon pole of the full $\mathcal{O}(q^3)$ IR CHPT partial wave and the direct (s -channel) Born term calculated with g_A , M_π and m at their physical values, gives us directly the ratio between the squares of the full pion-nucleon coupling and the one from the GT relation.^{#5} Numerically we find that the full calculation gives rise to a violation of the GT relation of around 20-25%, while its strict $\mathcal{O}(M_\pi^3)$ restriction is much smaller, eq. (3.10). Related to this one has a significant renormalization scale dependence on the GT violation.^{#6} In this way, for the fit KA85-1 (second column of Table 1) at $\lambda = 1$ GeV one has a 22% of violation of the GT relation while for $\lambda = 0.5$ GeV a 15% stems. On the other hand, ref. [4] performed a relativistic calculation of Δ_{GT} directly in dimensional regularization within the $\overline{MS} - 1$ renormalization scheme and obtained a natural (much smaller) and renormalization scale independent loop contribution to Δ_{GT} . It seems then that the problem that we find for the calculation of Δ_{GT} with IR, obtained earlier in ref. [27], is related to the peculiar way the chiral counting is restored in the IR approach [64, 65]. We tentatively conclude that a neat advance in the field would occur once a relativistic regularization method were available that conserved the chiral counting in the evaluation of loops while, at least, avoided any residual renormalization scale dependence.

4 Unitarized amplitudes and higher energies

In order to resum the right-hand cut or unitarity cut we consider the unitarization method of refs. [31, 32], to which we refer for further details. Notice that this method does not only provide a unitary πN amplitude but also takes care of the analyticity properties associated with the right-hand cut. In ref. [31] this approach was used for unitarizing the $\mathcal{O}(q^3)$ HBCHPT πN partial waves from ref. [16]. However, no explicit Lorentz-invariant one-loop calculation for πN scattering has been unitarized in the literature yet. This is an interesting point since by taking explicitly into account the presence of the unitarity cut the rest of the amplitude is expected to have a softer chiral expansion. According to ref. [32] we express $\mathcal{T}_{IJ\ell}$ as

$$T_{IJ\ell} = \frac{1}{\mathcal{T}_{IJ\ell}^{-1} + g(s)}, \quad (4.1)$$

^{#5}Note that there is no crossed Born term for $\pi^- p \rightarrow \pi^- p$ and that the LO Born term in term of physical parameters satisfies exactly the GT relation.

^{#6}Eq. (3.10) is renormalization scale independent because the beta function for d_{18} is zero [16].

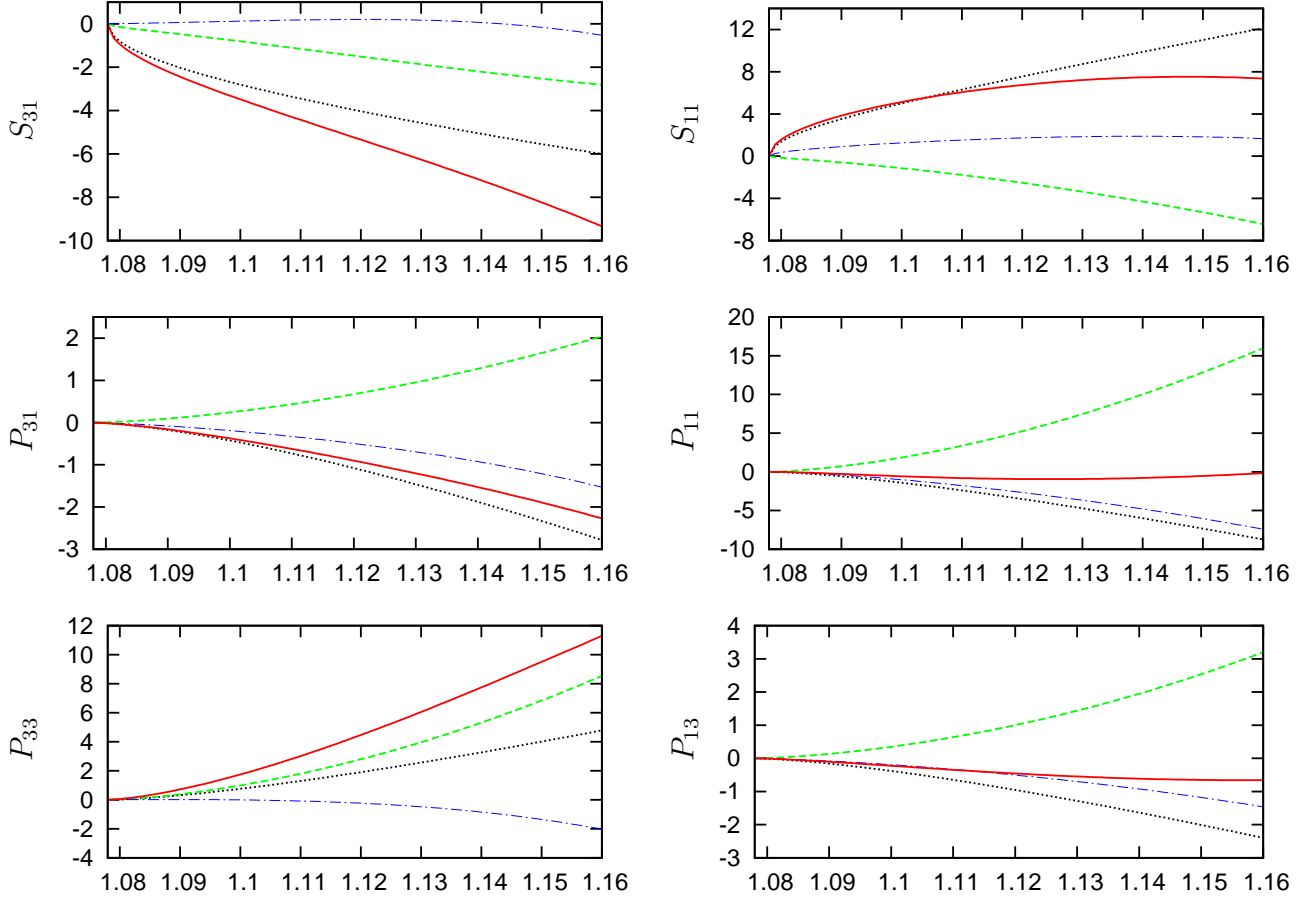


Figure 4: (Color online.) Different chiral orders contributing to the phase shifts for the KA85-1 fit. The (black) dotted, (green) dashed and (blue) dash-dotted are the first, second and third order, respectively. The (red) solid line is the sum of all of them.

where the unitarity pion-nucleon loop function is given by

$$\begin{aligned}
g(s) = \frac{1}{(4\pi)^2} \left\{ a_1 + \log \frac{m^2}{\mu^2} - \frac{M_\pi^2 - m^2 + s}{2s} \log \frac{m^2}{M_\pi^2} + \frac{|\mathbf{p}|}{\sqrt{s}} \left[\log(s - \Delta + 2\sqrt{s}|\mathbf{p}|) \right. \right. \\
\left. \left. + \log(s + \Delta + 2\sqrt{s}|\mathbf{p}|) - \log(-s + \Delta + 2\sqrt{s}|\mathbf{p}|) - \log(-s - \Delta + 2\sqrt{s}|\mathbf{p}|) \right] \right\}, \quad (4.2)
\end{aligned}$$

with $\Delta = M_\pi^2 - m^2$. The interaction kernel $\mathcal{T}_{IJ\ell}$ has no right-hand cut and is determined by matching order by order with the perturbative chiral expansion of $T_{IJ\ell}$ calculated in CHPT. In this way, with $g(s) = \mathcal{O}(q)$, one has [32]

$$T_{IJ\ell}^{(1)} + T_{IJ\ell}^{(2)} + T_{IJ\ell}^{(3)} = \mathcal{T}_{IJ\ell}^{(1)} + \mathcal{T}_{IJ\ell}^{(2)} + \mathcal{T}_{IJ\ell}^{(3)} - g(s) \left(T_{IJ\ell}^{(1)} \right)^2, \quad (4.3)$$

so that

$$\begin{aligned}
\mathcal{T}_{IJ\ell}^{(1)} &= T_{IJ\ell}^{(1)} , \\
\mathcal{T}_{IJ\ell}^{(2)} &= T_{IJ\ell}^{(2)} , \\
\mathcal{T}_{IJ\ell}^{(3)} &= T_{IJ\ell}^{(3)} + g(s) \left(T_{IJ\ell}^{(1)} \right)^2 ,
\end{aligned} \tag{4.4}$$

and $\mathcal{T}_{IJ\ell} = \mathcal{T}_{IJ\ell}^{(1)} + \mathcal{T}_{IJ\ell}^{(2)} + \mathcal{T}_{IJ\ell}^{(3)}$ is then replaced in eq. (4.1). Since the resulting partial wave is now unitary, we calculate the phase shifts directly from the relation $T_{IJ\ell} = \frac{8\pi\sqrt{s}}{|\mathbf{p}|} e^{i\delta_{IJ\ell}} \sin \delta_{IJ\ell}$ that follows from eqs. (2.15) and (2.16).

The subtraction constant a_1 is determined by requiring that $g(s)$ vanishes at the nucleon mass $s = m^2$. In this way the P_{11} partial-wave has the nucleon pole at its right position, otherwise it would disappear. This is due to the fact that for this partial wave $\mathcal{T}_{\frac{1}{2}\frac{1}{2}1}^{-1}$ vanishes at $s = m^2$ so it is required that $g(m^2) = 0$. Otherwise $T_{\frac{1}{2}\frac{1}{2}1}$, eq. (4.1), would be finite at $s = m^2$.

Due to the closeness of the $\Delta(1232)$ resonance to the πN threshold it is expedient to implement a method to take into account its presence in order to provide a higher energy description of πN phase-shifts beyond the purely perturbative results discussed in section 3. As commented in the introduction we can add a CDD pole [36] in the P_{33} channel so as to reach the region of the $\Delta(1232)$ resonance. The addition of the CDD pole conserves the discontinuities of the partial wave amplitude across the cuts. A CDD pole corresponds to a zero of the partial wave-amplitude along the real axis and hence to a pole in the inverse of the amplitude. We then modify eq. (4.1) by including such a pole in $T_{\frac{3}{2}\frac{3}{2}1}^{-1}$,

$$T_{\frac{3}{2}\frac{3}{2}1} = \left(\mathcal{T}_{\frac{3}{2}\frac{3}{2}1}^{-1} + \frac{\gamma}{s - s_P} + g(s) \right)^{-1} , \tag{4.5}$$

where γ and s_P are the residue and pole position of the CDD pole, in order, so that two new free parameters enter. The amplitude $\mathcal{T}_{IJ\ell}$ is determined as in eq. (4.4). We also distinguish here between the fits to the KA85 [45] and WI08 [46] phase-shifts. The fits are done up to $\sqrt{s} = \sqrt{s}_{max} = 1.25$ GeV for all the partial waves. One cannot afford to go to higher energies because of an intrinsic limitation of IR CHPT. Additional unphysical cuts and poles are generated by the infinite order resummation of the sub-leading $1/m$ kinetic energy terms accomplished in IR [64, 65, 14]. In our case the limiting circumstance is the appearance of a pole when the Mandelstam variable $u = 0$.^{#7} When projecting in the different partial waves this singularity gives rise to a strong branch point at $s = 2(m^2 + M_\pi^2) \simeq 1.34^2$ GeV², which indicates the onset of a non-physical right-hand cut that extends to infinity and that produces strong violation of unitarity. This translates into strong rises of the phase-shifts calculated employing eq. (4.5) for energies $\sqrt{s} \gtrsim 1.26$ GeV. This is why we have taken $\sqrt{s}_{max} = 1.25$ GeV because for higher energies these effects are clearly visible in the calculated phase-shifts. The χ^2 to be minimized is the same as already used for the pure perturbative study, eq. (3.5), employing also the same definition for

^{#7}Many of the tensor integrals involved in the one-loop calculations of πN scattering develop such a pole. In particular, it arises in the simplest scalar two-point loop function $I(u)$, following the notation of ref. [8].

$\text{err}(\delta)$. The resulting fits are shown in fig. 5, where the solid lines correspond to the fit of the KA85 data and the dashed ones to WI08. One can see a rather good agreement with data in the whole energy range from threshold up to 1.25 GeV, including the reproduction of the raise in the P_{33} phase shifts associated with the $\Delta(1232)$ resonance. The improvement is manifest in the P_{11} partial wave although some discrepancy with the WI08 data in the lower energy region remains, being better the agreement with KA85 phase-shifts. Compared with the perturbative treatment of section 3 one observes a drastic increase in the range of energies for which a globally acceptable description of the data is achieved.

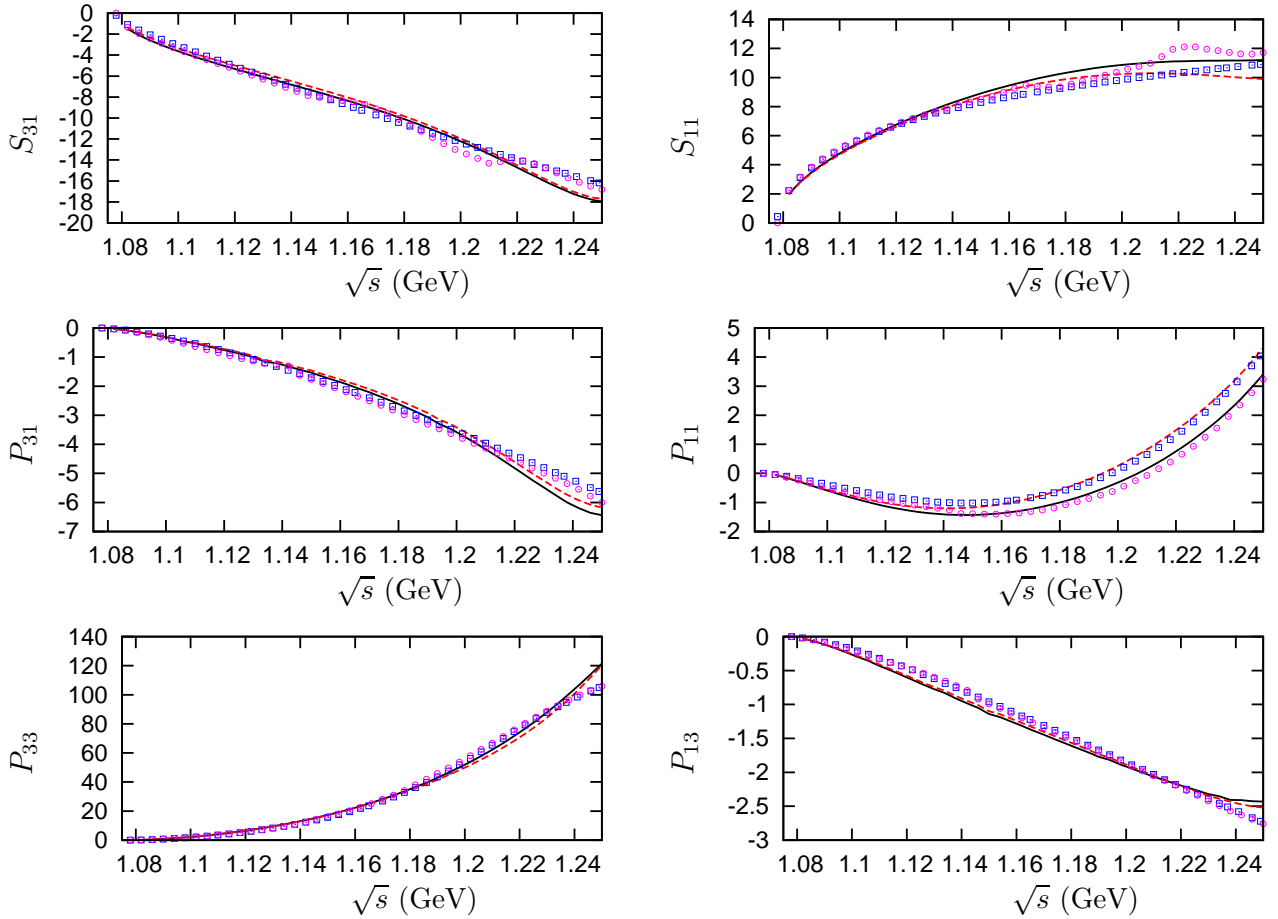


Figure 5: (Color online.) Fits to the KA85 and WI08 pion-nucleon phase shifts as a function of \sqrt{s} (in GeV) employing the unitarized πN amplitudes, eq. (4.5). The solid (dashed) lines correspond to the fit of the KA85 (WI08) data.

The values of the resulting LECs are collected in Table 5. We consider that the pure perturbative study of section 3 is the proper way to determine the chiral LECs. The new values in Table 5 do not constitute an alternative determination to those offered in Tables 1 and 3 and should be employed within UCHPT studies. Nonetheless, it is remarkable that the values for the LECs obtained are compatible with the average of values given in the fourth column of Table 3, in particular, for the $\mathcal{O}(q^2)$ LECs the central values are also rather close to the fitted values in

Table 5. Since we have a procedure to generate the $\Delta(1232)$ resonance through the CDD pole in eq. (4.5), such agreement is surprising since the contribution of this resonance to the LECs is very important [50]. The point is that the typical value of $\gamma/(s - s_P)$ in the low-energy region studied in section 3 is only around a factor 2 larger in modulus than the subtraction constant $a_1/(4\pi)^2$ in eq. (4.2), being the latter a quantity of first chiral order. As a result, at low energies, the CDD pole gives a contribution that can be computed as $\mathcal{O}(q^3)$, since the lowest order ones comes from $-(T_{IJL}^{(1)})^2\gamma/(s - s_P)$. This explains why the values of the second order LECs are preserved, despite having included the CDD pole.

LEC	Fit KA85	Fit WI08	Partial Wave	Fit KA85	Fit WI08
c_1	-0.48 ± 0.51	-0.53 ± 0.48	$a_{S_{31}}$	-0.115	-0.104
c_2	4.62 ± 0.27	4.73 ± 0.30	$a_{S_{11}}$	0.152	0.150
c_3	-6.16 ± 0.27	-6.41 ± 0.29	a_{0+}^+	-0.026	-0.020
c_4	3.68 ± 0.13	3.81 ± 0.16	a_{0+}^-	0.089	0.085
$d_1 + d_2$	2.55 ± 0.60	2.70 ± 0.65	$a_{P_{31}}$	-0.050	-0.048
d_3	-1.61 ± 1.01	-1.73 ± 1.04	$a_{P_{11}}$	-0.080	-0.075
d_5	0.93 ± 2.40	1.13 ± 2.18	$a_{P_{33}}$	0.245	0.250
$d_{14} - d_{15}$	-0.46 ± 1.00	-0.61 ± 1.11	$a_{P_{13}}$	-0.41	-0.039
d_{18}	0.01 ± 0.21	-0.03 ± 0.20			

Table 5: Fitted LECs in units GeV^{-1} (c_i) and GeV^{-2} (d_i) for the fits KA85 and WI08 employing the unitarized partial waves. We also give the scattering lengths and volumes in units of M_π and M_π^{-3} , respectively.

The values of the resulting threshold parameters with the present unitarized amplitudes are collected in the last two columns of Table 5. We observe that all of them are compatible with the averaged values given in the last column of Table 4. The P_{33} scattering volume turns out a bit too high in the lines of the values obtained with the perturbative fits following strategy 1, despite the reproduction of the $\Delta(1232)$ resonance. Finally, we also mention that similarly huge values for the GT violation are also obtained from the unitarized amplitudes as in the pure perturbative treatment. Indeed, the same value for Δ_{GT} , eq. (3.9), is obtained in the unitarized case for the same values of the LECs because $g(m^2) = 0$ (there is no CDD pole in the P_{11} partial wave.)

5 Summary and conclusions

We studied elastic pion-nucleon scattering employing covariant CHPT up-to-and-including $\mathcal{O}(q^3)$ in Infrared Regularization [8]. We followed two strategies for fitting the phase shifts provided the partial wave analysis of refs. [45, 46]. In one of them, instead of fitting the P_{33} phase-shifts, we considered the reproduction of the function $|\mathbf{p}|^3/\tan\delta_{P_{33}}$ around the threshold region (for $\sqrt{s} \leq 1.09$ GeV.) The rationale behind this is to reduce the impact of the $\Delta(1232)$ when performing fits to data, avoiding the rapid rise of phase-shifts with energy that tends to increase the value of the resulting scattering volume. An accurate reproduction of pion-nucleon phase-shifts up to

around 1.14 GeV results. The main difference between both strategies has to do with the values of the $\mathcal{O}(q^2)$ LECs c_2 and c_3 , that are smaller in absolute value for strategy 2 fits. As expected, the P_{33} scattering volume is also smaller for these fits and compatible with previous determinations. We have discussed separately the fits to data of the Karlsruhe [45] and GWU [46] groups. We obtain a much better reproduction of the P_{11} phase shifts for the former partial wave analysis. IR CHPT at $\mathcal{O}(q^3)$ is not able to reproduce the P_{11} phase shifts of the current solution of the GWU group even at very low energies. This suggests that a revision of this solution would be in order. The averaged values for the LECs and threshold parameters resulting from the two strategies and all data sets are given in the last columns of Tables 4 and 3 in good agreement with other previous determinations. The reproduction of experimental phase-shifts is similar in quality to that obtained previously with $\mathcal{O}(q^3)$ HBCHPT [16], showing also a smooth onset of the departure from experimental data for higher energies. This is an improvement compared with previous work [27]. In addition, we obtain a small violation of the Goldberger-Treiman relation at strict $\mathcal{O}(M_\pi^3)$, compatible with present determinations. However, the deviation from the Goldberger-Treiman relation is still a caveat because when all the terms in the full IR CHPT calculation at $\mathcal{O}(q^3)$ are kept the resulting discrepancy is much higher, around 20-30%.

We have also employed the non-perturbative methods of Unitary CHPT [32, 31] to resum the right-hand cut of the pion-nucleon partial waves. The $\Delta(1232)$ resonance is incorporated in the approach as a Castillejo-Dalitz-Dyson pole in the inverse of the amplitude. A good reproduction of the phase shifts is reached for \sqrt{s} up to around 1.25 GeV. There is an intrinsic limitation in IR CHPT for reaching higher energies due to the presence of a branch cut at $s = 2(m^2 + M_\pi^2) \simeq 1.34^2 \text{ GeV}^2$. Above that energy strong violations of unitarity occurs due to the onset of an unphysical cut associated with the infinite resummation of relativistic corrections accomplished in IR. This also originates a strong rise of phase-shifts noticeable already for $\sqrt{s} \gtrsim 1.25 \text{ GeV}$. The values of the LECs at $\mathcal{O}(q^2)$ is compatible to those obtained with the pure perturbative study.

Acknowledgements

We thank R. Workman for useful correspondence in connection with GWU group partial-wave analyses and SAID program. This work is partially funded by the grants MEC FPA2007-6277, FPA2010-17806 and the Fundación Séneca 11871/PI/09. We also thank the financial support from the BMBF grant 06BN411, the EU-Research Infrastructure Integrating Activity “Study of Strongly Interacting Matter” (HadronPhysics2, grant n. 227431) under the Seventh Framework Program of EU and the Consolider-Ingenio 2010 Programme CPAN (CSD2007-00042). JMC acknowledges the MEC contract FIS2006-03438, the EU Integrated Infrastructure Initiative Hadron Physics Project contract RII3-CT-2004-506078 and the Science and Technology Facilities Council [grant number ST/H004661/1] for support.

References

- [1] S. Weinberg, *Physica A* **96** (1979) 327.
- [2] J. Gasser and H. Leutwyler, *Annals Phys.* **158** (1984) 142.

- [3] S. R. Coleman, J. Wess and B. Zumino, Phys. Rev. **177** (1969) 2239; C. G. Callan, S. R. Coleman, J. Wess and B. Zumino, Phys. Rev. **177** (1969) 2247.
- [4] J. Gasser, M. E. Sainio and A. Svarc, Nucl. Phys. B **307** (1988) 779.
- [5] E. E. Jenkins and A. V. Manohar, Phys. Lett. B **255** (1991) 558.
- [6] V. Bernard, N. Kaiser, J. Kambor and U. G. Meissner, Nucl. Phys. B **388** (1992) 315.
- [7] V. Bernard, N. Kaiser and U. G. Meissner, Int. J. Mod. Phys. E **4** (1995) 193.
- [8] T. Becher and H. Leutwyler, Eur. Phys. J. C **9** (1999) 643.
- [9] P. J. Ellis and H. B. Tang, Phys. Rev. C **57** (1998) 3356.
- [10] J. L. Goity, D. Lehmann, G. Prezeau and J. Saez, Phys. Lett. B **504** (2001) 21; D. Lehmann and G. Prezeau, Phys. Rev. D **65**, 016001 (2001).
- [11] M. R. Schindler, J. Gegelia and S. Scherer, Phys. Lett. B **586** (2004) 258; M. R. Schindler, J. Gegelia and S. Scherer, Nucl. Phys. B **682**, 367 (2004).
- [12] J. Gegelia and G. Japaridze, Phys. Rev. D **60**, 114038 (1999).
- [13] T. Fuchs, J. Gegelia, G. Japaridze and S. Scherer, Phys. Rev. D **68**, 056005 (2003).
- [14] V. Bernard, Prog. Part. Nucl. Phys. **60** (2008) 82.
- [15] M. Mojzis, Eur. Phys. J. C **2** (1998) 181.
- [16] N. Fettes, U. G. Meissner and S. Steininger, Nucl. Phys. A **640** (1998) 199.
- [17] N. Fettes and U. G. Meissner, Nucl. Phys. A **676** (2000) 311.
- [18] N. Fettes and U. G. Meissner, Nucl. Phys. A **679** (2001) 629.
- [19] T. R. Hemmert, B. R. Holstein and J. Kambor, Phys. Lett. B **395** (1997) 89.
- [20] N. Fettes and U. G. Meissner, Nucl. Phys. A **679** (2001) 629.
- [21] V. Pascalutsa and D. R. Phillips, Phys. Rev. C **67** (2003) 055202; V. Pascalutsa, M. Vanderhaeghen and S. N. Yang, Phys. Rep. **437** (2007) 125; V. Pascalutsa, Prog. Part. Nucl. Phys. **61** (2008) 27.
- [22] B. Long and U. van Kolck, Nucl. Phys. A **840** (2010) 39.
- [23] J. Gasser, M. A. Ivanov, E. Lipartia, M. Mojzis and A. Rusetsky, Eur. Phys. J. C **26** (2002) 13.
- [24] M. Hoferichter, B. Kubis and U. G. Meissner, Phys. Lett. B **678** (2009) 65.
- [25] J. Gasser, V. E. Lyubovitskij and A. Rusetsky, Ann. Rev. Nucl. Part. Sci. **59**, 169 (2009).

- [26] T. Becher and H. Leutwyler, JHEP **0106** (2001) 017.
- [27] K. Torikoshi and P. J. Ellis, Phys. Rev. C **67** (2003) 015208.
- [28] M. L. Goldberger and S. B. Treiman, Phys. Rev. **110** (1958) 1178.
- [29] J. A. Oller and E. Oset, Nucl. Phys. A **620**, 438 (1997); (E)-ibid. A **652**, 407 (1999)].
- [30] J. A. Oller and E. Oset, Phys. Rev. D **60**, 074023 (1999).
- [31] U. G. Meissner and J. A. Oller, Nucl. Phys. A **673**, 311 (2000).
- [32] J. A. Oller and U. G. Meissner, Phys. Lett. B **500**, 263 (2001).
- [33] A. Gómez Nicola, J. Nieves, J. R. Peláez and E. R. Arriola, Phys. Rev. D **69** (2004) 076007.
- [34] J. Nieves and E. Ruiz Arriola, Phys. Rev. D **63** (2001) 076001.
- [35] A. Gasparyan and M. F. M. Lutz, arXiv:1003.3426 [hep-ph].
- [36] L. Castillejo, R. H. Dalitz and F. J. Dyson, Phys. Rev. **101** (1956) 453.
- [37] G. F. Chew, “The Analytic S -Matrix”. W. A. Benjamin, Inc. New York, 1966.
- [38] P. D. B. Collins, “Regge theory and high energy physics”. Cambridge University Press, New York, 1977.
- [39] V. Bernard, N. Kaiser, U. G. Meissner and A. Schmidt, Z. Phys. A **348** (1994) 317.
- [40] B. Borasoy and U. G. Meissner, Annals Phys. **254**, 192 (1997).
- [41] G. Höler, “Pion-nucleon scattering”, edited by H. Schopper, Landolt-Börnstein, New Series, Group I, Vol. 9, Pt. B2 (Springer-Verlag, Berlin, 1983).
- [42] S. Weinberg, Phys. Lett. B **251** (1990) 288; Nucl. Phys. B **363** (1991) 3.
- [43] J. A. Oller, M. Verbeni and J. Prades, JHEP **0609** (2006) 079.
- [44] B. Kubis and U. G. Meissner, Nucl. Phys. A **679** (2001) 698.
- [45] R. Koch, Nucl. Phys. A **448** (1986) 707; R. Koch and E. Pietarinen, Nucl. Phys. A **336** (1980) 331.
- [46] Computer code SAID, online program at <http://gwdac.phys.gwu.edu/~>, solution WI08. R. A. Arndt *et al.*, Phys. Rev. C **74** (2006) 045205. solution SM01.
- [47] N. Fettes and U.-G. Meißner, Nucl. Phys. A **693** (2001) 693.
- [48] F. James, Minuit Reference Manual D **506** (1994).
- [49] P. Buettiker and U. G. Meissner, Nucl. Phys. A **668** (2000) 97.

- [50] V. Bernard, N. Kaiser and U.-G. Meißner, Nucl. Phys. A **615** (1997) 483.
- [51] J. Gasser, V. E. Lyubovitskij and A. Rusetsky, Phys. Rep. **456** (2008) 167.
- [52] R. A. Arndt, W. J. Briscoe, I. I. Strakovsky, R. L. Workman, M. M. Pavan, Phys. Rev. C **69** (2004) 035213.
- [53] N. Kaiser, R. Brockmann and W. Weise, Nucl. Phys. A **625** (1997) 758.
- [54] E. Epelbaum, W. Glöckle and U.-G. Meißner, Eur. Phys. A **19** (2004) 125.
- [55] E. Epelbaum, W. Glöckle and U.-G. Meißner, Eur. Phys. A **19** (2004) 401.
- [56] E. Epelbaum, A. Nogga, W. Glöckle, H. Kamada, U.-G. Meißner and H. Witala, Eur. Phys. J A **15** (2002) 543.
- [57] M. C. M. Rentmeester, R. G. E. Timmermans and J. J. de Swart, Phys. Rev. C **67** (2003) 044001.
- [58] M. C. M. Rentmeester, R. G. E. Timmermans, J. L. Friar, J. J. de Swart, Phys. Rev. Lett. **82** (1999) 4992.
- [59] R. A. Arndt, W. J. Briscoe, I. I. Strakovsky, R. L. Workman, Phys. Rev. C **74** (2006) 045205.
- [60] U.-G. Meißner, U. Raha and A. Rusetsky, Phys. Lett. B **639** (2006) 478.
- [61] R. A. Arndt, R. L. Workman and M. M. Pavan, Phys. Rev. C **49** (1994) 2729.
- [62] H.-Ch. Schröder *et al.*, Eur. Phys. J. C **21** (2001) 473.
- [63] J. J. de Swart, M. C. M. Rentmeester and R. G. E. Timmermans, πN Newsletter **13** (1997) 96.
- [64] B. R. Holstein, V. Pascalutsa and M. Vanderhaeghen, Phys. Rev. D **72** (2005) 094014.
- [65] L. S. Geng, J. Martin Camalich, L. Alvarez-Ruso and M. J. Vicente-Vacas, Phys. Rev. Lett. **101** (2008) 222002.